Dipole and quadrupole transition strengths in Ba^+ from measurements of K splittings in high-L barium Rydberg levels

Shannon L. Woods and S. R. Lundeen
Colorado State University, Fort Collins, Colorado 80523, USA

Erica L. Snow
SUNY Fredonia, Fredonia, New York 14063, USA

(Received 27 July 2009; published 27 October 2009)

Measurements of K splittings in high-L Rydberg states of barium are used to deduce electric-dipole and electric-quadrupole matrix elements in Ba^+. The model used to interpret these splittings is extended here to include the contributions of third- and fourth-order perturbation terms, altering the conclusions of a previous report that omitted those contributions. The analysis leads to improved experimental determinations of dipole ($6s$-$6p$) and quadrupole ($6s$-$5d$) transition strengths in Ba^+ that are in good agreement with recent *a priori* calculations.

DOI: 10.1103/PhysRevA.80.042516 PACS number(s): 32.70.Cs, 32.10.Fn, 32.10.Dk

I. INTRODUCTION

Knowledge of atomic and ionic transition strengths is necessary in a very wide range of applications. Some applications, such as ultraprecise atomic clocks [1] and tests of fundamental interaction strengths [2], require the highest possible precision. In contrast to atomic binding energies, which are often tabulated precisely from spectroscopic studies [3], transition strengths must be calculated. The accuracy of these calculations is difficult to assess without experimental tests. Atomic and ionic lifetime measurements, of course, provide one of the best tests of these calculations. Depending on the magnitude of the lifetime and ionization state, many different experimental techniques have been used to measure both allowed and forbidden lifetimes in a variety of atoms and ions [4]. Another common source of sensitive tests, but only for positive ions, is the study of fine structure in high-L Rydberg states [5]. The binding energies of nonpenetrating high-L Rydberg electrons are sensitive to the dipole and quadrupole polarizabilities of the positive ion binding them in their orbit, and these in turn depend on many of the same matrix elements that determine excited-state lifetimes.

The Ba^+ ion presents an additional unique opportunity to obtain precise experimental tests of calculated transition probabilities. The high-L Rydberg states of barium display prominent splittings between the two states differing in the relative orientation of the $^2S_{1/2}$ Ba^+ ion and the nL Rydberg electron [6]. These two levels are characterized by the value of the intermediate quantum number K,

$$\vec{K} \equiv \vec{J}_C + \vec{L}, \tag{1}$$

where J_C is the angular momentum of the ion core and L is the angular momentum of the Rydberg electron. The energy difference between these two levels, the so-called K splittings, has been shown to be due to the indirect effect of spin-orbit splittings in the excited states of Ba^+ [7]. Measurements of the K splittings across a range of high-L Rydberg levels may be used to deduce electric-dipole and -quadrupole transition strengths connecting the Ba^+ ground state to the first-excited P and D levels [8]. To date, this technique has not been applied to any other positive ion, but future studies should be possible in other cases. Since lifetime, polarizability, and K-splitting measurements all exist for Ba^+, comparing the results obtained from these different experimental methods to *a priori* calculations should provide a valuable test of experimental and theoretical methods.

Figure 1 illustrates the lowest five levels of the Ba^+ ion, the $6s$ ground state, and the $5d$ and $6p$ excited levels. The electric-dipole and electric-quadrupole transitions between these levels are indicated. Since the energies of these levels are all precisely known, calculations of transition strengths are reduced to evaluation of matrix elements of electric-dipole and -quadrupole operators between calculated wave functions for the various levels. Table I shows one example of such calculated matrix elements, obtained using relativistic many-body perturbation-theory methods [9]. Measurements of the lifetime of all four excited states exist with precision between 1% and 10% [10–12]. Table II illustrates the good agreement between the most recent of these measurements and the predictions implied by the matrix elements of Table I [9]. Measurements of Rydberg fine structure in barium, i.e., of the $\Delta n=0$, $\Delta L=1$ energy splittings, have also been reported, from which values of the dipole and quadrupole polarizabilities of the $6s$ ground state can be determined [13]. Again, the most recent of these determinations, shown in Table II, are in good agreement with the predictions obtained from the matrix elements of Table I. Of course, these predictions must also take account of other fac-

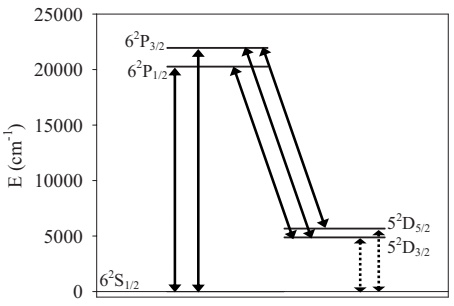

FIG. 1. Level diagram showing the lowest five levels of Ba^+. Solid arrows show the dipole transitions while the dotted arrows show the quadrupole transitions.

TABLE I. Calculated electric-dipole and -quadrupole matrix elements between the lowest five levels of the Ba^+ ion from Ref. [9]. All values are in atomic units.

Quantity	Value
$\langle 6S_{1/2}\|D\|6P_{1/2}\rangle$	3.3357
$\langle 6S_{1/2}\|D\|6P_{3/2}\rangle$	4.7065
$\langle 6S_{1/2}\|Q\|5D_{3/2}\rangle$	12.63(9)
$\langle 6S_{1/2}\|Q\|5D_{5/2}\rangle$	15.8(1)
$\langle 6P_{1/2}\|D\|5D_{3/2}\rangle$	3.034
$\langle 6P_{3/2}\|D\|5D_{3/2}\rangle$	1.325
$\langle 6P_{3/2}\|D\|5D_{5/2}\rangle$	4.080

tors, including the contributions from coupling to higher-excited states and the polarizability of the closed-shell Ba^{2+} core [9].

In contrast to the close correspondence between experiment and theory represented by Table II, the transition strengths derived from K splittings [8] show mixed agreement with these same calculations, as illustrated in Table III. The dipole matrix element agrees well with calculations, but the reported quadrupole matrix element differs by 30%, well outside of the uncertainty. This apparent discrepancy is confirmed by expansion of the data set to include additional measurements of K splittings in higher L levels reported recently [13]. We show below, however, that this conclusion is based on an incomplete model of the origin of the K splittings that includes only second-order perturbation terms. When the model is extended to include third- and fourth-order terms, close agreement with calculated dipole and quadrupole transition strengths is found.

Section II of this report describes the theoretical model of the K splittings, including calculations of third- and fourth-order contributions and compares the model's prediction to existing measurements. Section III considers the slight adjustments in the calculated matrix elements that are required to achieve full agreement with the measurements. The constraints on transition strengths derived from Rydberg K-splitting measurements are found to complement the constraints derived from polarizability measurements. Together, these two types of barium Rydberg data lead to improved

TABLE II. Comparison of measured Ba^+ lifetimes and polarizabilities to values calculated using the matrix elements of Table I.

Quantity	Expt.	Theor.[a]	(Expt.)/(Theor.)
$\tau(6\,^2P_{1/2})$	7.90(10) ns[b]	7.83	1.009(13)
$\tau(6\,^2P_{3/2})$	6.32(10) ns[b]	6.27	1.008(16)
$\tau(5\,^2D_{3/2})$	79.8(4.6) s[c]	81.5(1.2)	0.98(6)
$\tau(5\,^2D_{5/2})$	32.0(4.6) s[d]	30.3(4)	1.06(15)
$\alpha_D(6\,^2S_{1/2})$	123.88(5) a.u.[e]	124.15	0.9978(4)
$\alpha_Q(6\,^2S_{1/2})$	4420(250) a.u.[e]	4182(34)	1.06(6)

[a]Reference [9].
[b]Reference [12].
[c]Reference [10].
[d]Reference [11].
[e]Reference [13].

TABLE III. Comparison of dipole and quadrupole matrix elements obtained in Ref. [8] from barium Rydberg K splittings to the calculated values shown in Table I. Since pure LS coupling was assumed in Ref. [9], a comparable value has been extracted from the matrix elements in Table I. All values are in atomic units.

Quantity	Expt.[a]	Theor.[b]	(Expt.)/(Theor.)
$\langle 6s\|D\|6p\rangle$	4.03(10)	4.08	0.99(3)
$\langle 6s\|Q\|5d\rangle$	9.76(29)	14.26(8)	0.68(2)

[a]Reference [8].
[b]Reference [9].

determinations of both dipole ($6s$-$6p$) and quadrupole ($6s$-$5d$) transition strengths.

II. THEORY OF K SPLITTINGS

A. Second-order model

A theoretical model of the K-splitting intervals emerges from the same formulation used to model the fine-structure pattern in nonpenetrating high-L Rydberg states. This formulation is based on a perturbation expansion of the interactions between a hydrogenic Rydberg electron and an isolated positive-ion core. These interactions are expressed in a multipole expansion

$$V = \sum_{\kappa=1}^{\infty} \sum_{i=1}^{N-1} \frac{r_i^{\kappa}}{r_N^{\kappa+1}} C^{[\kappa]}(\hat{r}_i) C^{[\kappa]}(\hat{r}_N). \tag{2}$$

The zeroth-order wave functions are products of the $N-1$ electron core eigenfunctions (n_c, L_c, J_c) and the one-electron Rydberg functions (n,L), coupled to form the angular momentum K. The spin of the Rydberg electron is ignored.

The first nonzero contributions to the perturbation energy come from second-order perturbation expressions. Including the first two multipole terms, the difference in energy between the $K=L\pm\frac{1}{2}$ levels is calculated to be

$$\delta E(n,L) \equiv E\left(n,L,K=L+\tfrac{1}{2}\right) - E\left(n,L,K=L-\tfrac{1}{2}\right) = \delta E_{DD} + \delta E_{QQ}, \tag{3}$$

where

$$\delta E_{DD} = -\sum_{n_c} \frac{\langle 6S_{1/2}\|\vec{D}\|n_c P_{1/2}\rangle^2}{6} [f_{nL}(L+1, E(n_c P_{1/2}), 2, 2) - f_{nL}(L-1, E(n_c P_{1/2}), 2, 2)] + \sum_{n_c} \frac{\langle 6S_{1/2}\|\vec{D}\|n_c P_{3/2}\rangle^2}{12} [f_{nL}(L+1, E(n_c P_{3/2}), 2, 2) - f_{nL}(L-1, E(n_c P_{3/2}), 2, 2)], \tag{4}$$

with

$$\vec{D} = \sum_{i}^{N-1} r_i C^{[1]}(\hat{r}_i) \tag{5}$$

and

$$\delta E_{QQ} = \frac{3}{2}\sum_{n_c}\frac{\langle 6S_{1/2}\|\vec{\vec{Q}}\|n_cD_{3/2}\rangle^2}{10}[g_+(L)f_{nL}(L + 2,E(n_cD_{3/2}),3,3) + g_0(L)f_{nL}(L,E(n_cD_{3/2}),3,3) + g_-(L)f_{nL}(L-2,E(n_cD_{3/2}),3,3)] - \sum_{n_c}\frac{\langle 6S_{1/2}\|\vec{\vec{Q}}\|n_cD_{5/2}\rangle^2}{10}[g_+(L)f_{nL}(L + 2,E(n_cD_{5/2}),3,3) + g_0(L)f_{nL}(L,E(n_cD_{5/2}),3,3) + g_-(L)f_{nL}(L-2,E(n_cD_{5/2}),3,3)], \quad (6)$$

with

$$\vec{\vec{Q}} = \sum_i^{N-1} r_i^2 C^{[2]}(\hat{r}_i), \quad g_+(L) = -\frac{(L+2)}{(2L+3)},$$

$$g_0(L) = \frac{(2L+1)}{(2L-1)(2L+3)}, \text{ and } g_-(L) = +\frac{(L-1)}{(2L-1)}. \quad (7)$$

In both expressions,

$$f_{nL}(L',E_C,s,q) \equiv \sum_{n'}\frac{\langle n,L|r^{-s}|n',L'\rangle\langle n',L'|r^{-q}|n,L\rangle}{E_C + E(n') - E(n)}, \quad (8)$$

where $E(n)$ and $E(n')$ are the hydrogenic energies of the Rydberg electron. In Eq. (8), the sum over n' implicitly includes continuum levels.

One important characteristic of the K splittings is easily seen from these expressions. If the core excitation energies are sufficiently large that the core responds adiabatically, i.e., if

$$\frac{1}{E_C + E(n') - E(n)} \cong \frac{1}{E_C}, \quad (9)$$

then completeness of the radial functions implies that

$$f_{nL}(L',E_C,s,q) = \frac{\langle r^{-(s+q)}\rangle_{nL}}{E_C} \quad (10)$$

and both dipole and quadrupole contributions to the K splittings vanish identically. Thus, a key feature of the K splittings is that they are a signature of nonadiabatic response of the core to perturbation by the Rydberg electron.

If the core excitation energies are not too small, it is possible to simplify the expressions above using the properties of hydrogenic radial functions. Taking

$$\frac{1}{E_C + E(n') - E(n)} = \frac{1}{E_C}\left(1 - \frac{E(n') - E(n)}{E_C} + \cdots\right) \quad (11)$$

and using

$$\sum_{n'}\langle n,L|r^{-s}|n',L'\rangle\langle n',L'|r^{-q}|n,L\rangle[E(n') - E(n)] = \frac{1}{2}[sq - L(L+1) + L'(L'+1)]\langle n,L|r^{-(s+q+2)}|n,L\rangle, \quad (12)$$

the K-splitting expressions can be simplified to the form

$$\delta E_{DD} = \frac{(2L+1)}{12}\langle r^{-6}\rangle_{nL}\sum_{n_c}\left(\frac{2\langle 6S_{1/2}\|\vec{D}\|n_cP_{1/2}\rangle^2}{E(n_cP_{1/2})^2} - \frac{\langle 6S_{1/2}\|\vec{D}\|n_cP_{3/2}\rangle^2}{E(n_cP_{3/2})^2}\right) \quad (13)$$

and

$$\delta E_{QQ} = \frac{(2L+1)}{20}\langle r^{-8}\rangle_{nL}\sum_{n_c}\left(\frac{3\langle 6S_{1/2}\|\vec{\vec{Q}}\|n_cD_{3/2}\rangle^2}{E(n_cD_{3/2})^2} - \frac{2\langle 6S_{1/2}\|\vec{\vec{Q}}\|n_cD_{5/2}\rangle^2}{E(n_cD_{5/2})^2}\right), \quad (14)$$

where only the first nonadiabatic terms have been included.

In this form, several features of the K splittings can be seen. First, if the energies of the $J_c = L_c \pm \frac{1}{2}$ core states are equal and the matrix elements to these two states are in the pure LS coupling ratio, then the K splittings vanish identically. This cancellation can be frustrated either by the fine-structure splittings or by a variation in the matrix element ratios, though the former is more significant in barium. For example, in pure LS coupling, the matrix element ratios would be

$$\frac{\langle 6S_{1/2}\|\vec{D}\|n_cP_{1/2}\rangle}{\langle 6S_{1/2}\|\vec{D}\|n_cP_{3/2}\rangle} = \sqrt{\frac{1}{2}}$$

$$\frac{\langle 6S_{1/2}\|\vec{\vec{Q}}\|n_cD_{3/2}\rangle}{\langle 6S_{1/2}\|\vec{\vec{Q}}\|n_cD_{5/2}\rangle} = \sqrt{\frac{2}{3}}. \quad (15)$$

The calculated matrix elements in Table I differ from these ratios by 0.2% and 2.1% for D and Q, respectively. By comparison, the excitation energies of the two fine-structure levels of $6p$ and $5d$ states differ by 8.3% and 16.4%.

If it is assumed that the matrix elements are in the LS ratio and the expressions are expanded to first order in the ratio of fine-structure splittings $\Delta E(n_c,L_c)$ to average excitation energies $E(n_c,L_c)$, the expressions can be further simplified to

$$\delta E_{DD} = \frac{2}{9}(2L+1)\langle r^{-6}\rangle_{nL}\sum_{n_c}\langle 6s\|\vec{D}\|n_cp\rangle^2\frac{\Delta E(n_cp)}{E(n_cp)^3} \quad (16)$$

and

TABLE IV. Comparison of evaluation of f_{nL} by the full calculation or by use of the adiabatic expansion. Columns 1–3 specify the particular f_{nL}. Column 4 shows the full result, obtained with the use of the Dalgarno-Lewis technique [15]. Columns 5 and 6 show the adiabatic and first nonadiabatic terms in the adiabatic expansion of f_{nL}. The ratio of the sum of f_0 and f_1 to the full result, shown in column 7, indicates the degree of convergence of the adiabatic expansion method. Column 8 shows the ratio of the average Rydberg energy difference to the core excitation energy, which should be a predictor of the degree of convergence.

nL	L'	Core state	f_{nL} 10^{-8} a.u.	f_0 10^{-8} a.u.	f_1 10^{-8} a.u.	$(f_0+f_1)/f_{nL}$	$\frac{(E(n')-E(n))_{AV}}{E_C}$
17,6	5	$6P_{3/2}$	27.797	25.793	1.818	0.993	−0.07
17,6	7	$6P_{3/2}$	22.643	25.793	−4.090	0.958	0.16
17,8	7	$6P_{3/2}$	6.6216	6.4189	0.2036	1.000	−0.03
17,8	9	$6P_{3/2}$	6.0728	6.4189	−0.3732	0.996	0.06
17,6	4	$5D_{5/2}$	0.53869	0.17583	0.11377	0.538	−0.65
17,6	6	$5D_{5/2}$	0.14603	0.17583	−0.07876	0.665	0.45
17,6	8	$5D_{5/2}$	0.076193	0.17583	−0.341311	−2.172	1.94
17,8	6	$5D_{5/2}$	0.018409	0.013128	0.003700	0.914	−0.28
17,8	8	$5D_{5/2}$	0.012130	0.013128	−0.001586	0.952	0.12
17,8	10	$5D_{5/2}$	0.0086361	0.013128	−0.008282	0.561	0.63

$$\delta E_{QQ} = \frac{6}{25}(2L+1)\langle r^{-8}\rangle_{nL}\sum_{n_c}\langle 6s\|\vec{Q}\|n_c d\rangle^2\frac{\Delta E(n_c d)}{E(n_c d)^3}. \quad (17)$$

These are the same equations reported by Snow *et al.* [7] and by Shuman and Gallagher [8]. This form has the advantage of displaying the rapidly decreasing influence of excited states above the lowest excitation of each L_c. Since both the matrix element and the fine-structure splitting decrease while the excitation energy increases, only the lowest P state, $6p$, and the lowest D state, $5d$, contribute significantly to the K splitting. This is similar to the dominant influence of the lowest states in calculations of polarizabilities, but much stronger. This form also shows that the relative importance of the QQ term decreases with L, as it is proportional to a higher inverse power of r. This allows the two contributions to be separately deduced from data that include a range of L.

Neither of the approximations used to derive Eqs. (16) and (17) above, the adiabatic expansion, and the expansion in $\Delta E/E$ are particularly good for the $5d$ level. The adiabatic expansion is particularly ineffective because of the very low excitation energy of the $5d$ levels. To illustrate this, Table IV shows the full value of f_{nL} [Eq. (8)] and the first two terms in its adiabatic expansion for typical values of f_{nL}. The specific cases are the $n=17$ levels with $L=6$ and 8 for $6P_{3/2}$ and $5D_{5/2}$ intermediate core states. The adiabatic term is from Eq. (10) while the first nonadiabatic term is calculated using Eqs. (11) and (12). The ratio of the sum of the adiabatic and first nonadiabatic terms to the full value is also shown, indicating good convergence for $6p$ levels, but nonconvergence for $5d$ levels. These examples also illustrate that evaluation of f_{nl} using the adiabatic expansion improves as L increases. A useful estimate of the utility of the adiabatic expansion is the estimation of the average Rydberg energy difference, obtained by using the appropriate squared radial matrix element as a weighting function [8]

$$[E(n')-E(n)]_{AV} \equiv \frac{\sum_{n'}\langle nL|r^{-s}|n'L'\rangle^2[E(n')-E(n)]}{\sum_{n'}\langle nL|r^{-s}|n'L'\rangle^2} = \frac{[s^2-L(L+1)+L'(L'+1)]}{2}\frac{\langle r^{-2(s+1)}\rangle_{nL}}{\langle r^{-2s}\rangle_{nL}}. \quad (18)$$

If the ratio of this average Rydberg energy difference to the core excitation energy is small, then the adiabatic expansion is likely to be useful. This ratio is also shown in Table IV for the example cases, confirming its predictive value. Because the $5d$ levels play a significant role in the barium K splittings, it is necessary to return to the full expressions of Eqs. (4) and (6) to evaluate the predicted K splittings.

Table V collects the measured K splittings in states with $L \geq 6$ [13,14] and compares them to this second-order model, evaluated using the theoretical matrix elements from Table I. These calculations truncate the summation over n_c to include only the $6p$ and $5d$ levels and evaluate the necessary sums in Eq. (8) using the Dalgarno-Lewis technique [15]. This approach has the advantage of naturally including the contributions of continuum Rydberg levels which are of particular significance when $L' > L$. Table V also indicates the small contributions of the "normal" magnetic spin splittings in the predicted K splittings

$$\delta E_N = \frac{-\alpha^2}{n^3 L(L+1)}\text{a.u.} \quad (19)$$

The excess of the measured values of K splittings over the normal magnetic splittings is in very poor agreement with the second-order model, as Table V illustrates. If one assumes that the poor agreement is due to the use of an incorrect quadrupole matrix element and adjusts the matrix ele-

TABLE V. Comparison of measured barium K splittings to the predictions of the second-order model using theoretical matrix elements from Table I and experimental term energies. Column 2 shows the measured values [13,14]. Column 3 shows the normal magnetic splitting. Columns 4 and 5 show the predicted contributions from dipole and quadrupole second-order terms. The observed value minus the normal magnetic splitting is shown in column 6 and the ratio of this to the prediction of the second-order model is shown in column 7. All values are in MHz.

nL	δE_{Obs}	δE_N	δE_{DD}	δE_{QQ}	$\delta E_{Obs}-\delta E_N$	$\frac{\delta E_{Obs}-\delta E_N}{\delta E_{\text{Theor.}}}$
9,6	721(9)	−11	491	452	733(9)	0.777(10)
9,7	137(9)	−9	125	31	145(9)	0.94(6)
10,6	640(6)	−8	402	475	648(6)	0.740(7)
10,7	131(9)	−6	109	32	137(9)	0.97(6)
17,6	261.67(10)	−1.70	107.37	312.22	263.37(10)	0.6277(2)
17,7	40.676(89)	−1.274	33.297	15.817	41.950(89)	0.854(2)
17,8	12.04(11)	−0.99	11.69	2.44	13.03(11)	0.922(8)
17,9	3.97(12)	−0.79	4.52	0.53	4.76(12)	0.943(24)
17,10	1.24(15)	−0.65	1.88	0.14	1.89(15)	0.94(7)
20,7	26.545(56)	−0.782	21.479	10.971	27.327(56)	0.842(2)
20,8	7.839(53)	−0.608	7.671	1.701	8.447(53)	0.901(6)
20,9	2.46(13)	−0.49	3.03	0.38	2.95(13)	0.865(38)
20,10	0.70(14)	−0.40	1.29	0.10	1.10(14)	0.79(10)
20,11	−0.06(15)	−0.33	0.59	0.03	0.27(15)	0.44(24)

ments to minimize the discrepancy, the result is similar to the conclusion presented in Table III. However, since this conclusion conflicts with the evidence from lifetime and polarizability measurements, another possibility is that the theoretical model of K splittings is incomplete.

B. Extended model

In considering possible extensions to the theoretical model of K splittings, several different approaches were explored:

(a) Inclusion of higher excited states of the Ba^+ ion.

(b) Inclusion of octupole terms in V.

(c) Inclusion of higher-order perturbation terms, third and fourth orders.

Item (a) was eliminated because it contributes less than 0.1% to the K splitting of $L \geq 6$ states of barium. The possible contributions of these higher levels are accurately represented by Eqs. (16) and (17), so it is not difficult to show that their contributions are negligible. Item (b) is also easily eliminated, since the lowest F level of Ba^+ is much higher in energy than either the $6p$ or $5d$ levels and has a much smaller fine-structure splitting. This leaves item (c) as the most probable source of additional contributions.

The third-order terms with the lowest multipole order are DDQ, DQD, and QDD. As for the case of second-order terms, it was verified that these terms do not contribute to the K splittings in the adiabatic limit. Evaluating the contribution of these expressions to the K splitting without approximation is made difficult by the two independent sums over the intermediate states. Whenever at least one of these states is a $(6p,n'L')$ level, however, Table IV shows that treating it adiabatically should be a good approximation. With the DDQ and QDD terms, for example, the $6p$ energy is treated adiabatically while the sum over the $(5d,n'L')$ levels is expressed using the full f_{nL} functions defined in Eq. (8), giving the result

$$\begin{aligned}\delta E_{QDD} = \delta E_{DDQ} = {} & \frac{\sqrt{10}}{40}\frac{\langle 6S_{1/2}\|\vec{Q}\|5D_{3/2}\rangle\langle 5D_{3/2}\|\vec{D}\|6P_{1/2}\rangle\langle 6P_{1/2}\|\vec{D}\|6S_{1/2}\rangle}{E(6P_{1/2})}[g_+(L)f_{nL}(L+2,E(5D_{3/2}),3,4) \\ & + g_0(L)f_{nL}(L,E(5D_{3/2}),3,4) + g_-(L)f_{nL}(L-2,E(5D_{3/2}),3,4)] \\ & + \frac{1}{40}\frac{\langle 6S_{1/2}\|\vec{Q}\|5D_{3/2}\rangle\langle 5D_{3/2}\|\vec{D}\|6P_{3/2}\rangle\langle 6P_{3/2}\|\vec{D}\|6S_{1/2}\rangle}{E(6P_{3/2})}[g_+(L)f_{nL}(L+2,E(5D_{3/2}),3,4) + g_0(L)f_{nL}(L,E(5D_{3/2}),3,4) \\ & + g_-(L)f_{nL}(L-2,E(5D_{3/2}),3,4)] + \frac{\sqrt{6}}{60}\frac{\langle 6S_{1/2}\|\vec{Q}\|5D_{5/2}\rangle\langle 5D_{5/2}\|\vec{D}\|6P_{3/2}\rangle\langle 6P_{3/2}\|\vec{D}\|6S_{1/2}\rangle}{E(6P_{3/2})}[g_+(L)f_{nL}(L+2,E(5D_{5/2}),3,4) \\ & + g_0(L)f_{nL}(L,E(5D_{5/2}),3,4) + g_-(L)f_{nL}(L-2,E(5D_{5/2}),3,4)]. \end{aligned} \tag{20}$$

In the case of the *DQD* term, both intermediate states yield to the adiabatic expansion shown in Eq. (12), giving the approximate result for the *K* splitting

$$\delta E_{DQD} = \frac{\sqrt{5}}{60}(2L+1)\langle 6S_{1/2}\|\vec{D}\|6P_{3/2}\rangle\langle 6P_{3/2}\|\overleftrightarrow{Q}\|6P_{3/2}\rangle \times\langle 6P_{3/2}\|\vec{D}\|6S_{1/2}\rangle\frac{1}{E(6P_{3/2})^3}\langle r^{-9}\rangle_{nL} - \frac{\sqrt{10}}{60}(2L+1) \times\langle 6S_{1/2}\|\vec{D}\|6P_{1/2}\rangle\langle 6P_{1/2}\|\overleftrightarrow{Q}\|6P_{3/2}\rangle\langle 6P_{3/2}\|\vec{D}\|6S_{1/2}\rangle \times\left(\frac{E(6P_{1/2})-2E(6P_{3/2})}{E(6P_{1/2})^2E(6P_{3/2})^2}\right)\langle r^{-9}\rangle_{nL}. \quad (21)$$

The next nonzero multipole term in the third-order perturbation energy is of order *QQQ*, two factors of r^{-1} smaller than the previous terms. Calculation of this term is not attempted here because it involves two intermediate levels of the $(5d,\ n'L')$ type. Table IV shows that the adiabatic expansion completely fails in this case and thus evaluation of the nonadiabatic portion of this term is much more difficult. A rough estimate of their contribution, using the inappropriate adiabatic expansion, suggests that this term is probably insignificant for levels with $L>6$.

The lowest multipole term in the fourth-order perturbation energies is *DDDD*. Again, it was confirmed that these terms give zero contribution to the *K* splittings in the adiabatic limit. Since the $5d$ intermediate states give the most significant nonadiabatic response, only terms with a $5d$ intermediate core level were included here. The two $6p$ intermediate levels were treated adiabatically and the resulting approximate expression for the fourth-order contribution to the *K* splittings is

$$\begin{aligned}\delta E_{DDDD} = &-\frac{1}{24}\frac{\langle 6S_{1/2}\|\vec{D}\|6P_{1/2}\rangle\langle 6P_{1/2}\|\vec{D}\|5D_{3/2}\rangle\langle 5D_{3/2}\|\vec{D}\|6P_{1/2}\rangle\langle 6P_{1/2}\|\vec{D}\|6S_{1/2}\rangle}{E(6P_{1/2})E(6P_{1/2})}[g_+(L)f_{nL}(L+2,E(5D_{3/2}),4,4)\\ &+g_0(L)f_{nL}(L,E(5D_{3/2}),4,4)+g_-(L)f_{nL}(L-2,E(5D_{3/2}),4,4)]\\ &-\frac{\sqrt{10}}{120}\frac{\langle 6S_{1/2}\|\vec{D}\|6P_{1/2}\rangle\langle 6P_{1/2}\|\vec{D}\|5D_{3/2}\rangle\langle 5D_{3/2}\|\vec{D}\|6P_{3/2}\rangle\langle 6P_{3/2}\|\vec{D}\|6S_{1/2}\rangle}{E(6P_{1/2})E(6P_{3/2})}[g_+(L)f_{nL}(L+2,E(5D_{3/2}),4,4)\\ &+g_0(L)f_{nL}(L,E(5D_{3/2}),4,4)+g_-(L)f_{nL}(L-2,E(5D_{3/2}),4,4)]\\ &-\frac{1}{240}\frac{\langle 6S_{1/2}\|\vec{D}\|6P_{3/2}\rangle\langle 6P_{3/2}\|\vec{D}\|5D_{3/2}\rangle\langle 5D_{3/2}\|\vec{D}\|6P_{3/2}\rangle\langle 6P_{3/2}\|\vec{D}\|6S_{1/2}\rangle}{E(6P_{3/2})E(6P_{3/2})}[g_+(L)f_{nL}(L+2,E(5D_{3/2}),4,4)\\ &+g_0(L)f_{nL}(L,E(5D_{3/2}),4,4)+g_-(L)f_{nL}(L-2,E(5D_{3/2}),4,4)]\\ &-\frac{1}{60}\frac{\langle 6S_{1/2}\|\vec{D}\|6P_{3/2}\rangle\langle 6P_{3/2}\|\vec{D}\|5D_{5/2}\rangle\langle 5D_{5/2}\|\vec{D}\|6P_{3/2}\rangle\langle 6P_{3/2}\|\vec{D}\|6S_{1/2}\rangle}{E(6P_{3/2})E(6P_{3/2})}[g_+(L)f_{nL}(L+2,E(5D_{5/2}),4,4)\\ &+g_0(L)f_{nL}(L,E(5D_{5/2}),4,4)+g_-(L)f_{nL}(L-2,E(5D_{5/2}),4,4)]. \quad (22)\end{aligned}$$

The contributions of these third- and fourth-order terms are found to be quite significant and together they account almost completely for the discrepancy seen in Table V between measured *K* splittings and the predictions of the second-order model. This is illustrated in Table VI, which shows the third- and fourth-order contributions to the same intervals, again calculated using theoretical matrix elements and experimental term energies. The extended theory, with no adjustable elements, agrees to within a couple of percent for most of these intervals. In particular, the severe disagreement for levels with $6\leq L\leq 8$ is virtually eliminated by the addition of these terms. The improved agreement is illustrated in Fig. 2, which shows all the reported measurements with $L\geq 6$ [13,14] and compares them to both the second-order model (dashed line) and the extended model (solid line). To illustrate all these measurements on the same plot, the scaling suggested by Eqs. (13) and (14) has been used. The vertical axis represents the ratio of the measured splitting less the "normal" magnetic contribution to the expectation value of $(2L+1)\langle r^{-6}\rangle_{nL}$ in the appropriate Rydberg level. This scaling removes most of the variation of the *K* splitting with *n* and *L*. The horizontal axis in Fig. 2 is the ratio of the expectation values of $\langle r^{-8}\rangle_{nL}$ and $\langle r^{-6}\rangle_{nL}$ in the level of interest. If Eqs. (13) and (14) described the *K* splittings, they would lie on a straight line in this scaled plot. Clearly, this is not the case.

The largest deviations from the extended theory occur for the highest *L* intervals at the far left of Fig. 2. These lie systematically below the theory, with the deviation from theory approximately a factor of 3 larger for the $n=20$ intervals than for the $n=17$ intervals. This strongly suggests that the reported intervals have been affected by Stark shifts that differ for the two *K* values. Reference [13] did not consider this possibility, even though it was known that stray electric fields were present causing significant Stark shifts to the measured fine-structure intervals. The degree to which Stark shifts are different for the two *K* levels of common *L* de-

TABLE VI. Comparison of measured barium K splittings to the predictions of the extended theoretical model, including the contributions of the most significant third- and fourth-order perturbation terms. Contributions are calculated using theoretical matrix elements from Table I and experimental term energies. Columns 2 and 3 show the calculated third- and fourth-order contributions. The total theory, including the second-order terms from Table V, is shown in column 4 and the ratio of the observed value minus the normal magnetic splitting to this total is shown in column 5. All values are in MHz.

nL	$\delta E^{[3]}$	$\delta E^{[4]}$	Total $\delta E_{\text{Theor.}}$	$\frac{\delta E_{Obs}-\delta E_N}{\delta E_{\text{Theor.}}}$
9,6	−257.9	33.3	718.5	1.02(1)
9,7	−13.0	1.2	143.5	1.01(6)
10,6	−270.8	35.5	641.0	1.01(1)
10,7	−14.2	1.4	128.9	1.07(7)
17,6	−174.42	23.33	268.50	0.9809(4)
17,7	−7.381	0.779	42.512	0.987(2)
17,8	−0.90	0.07	13.30	0.980(8)
17,9	−0.16	0.01	4.91	0.971(24)
17,10	−0.03	0.00	1.98	0.95(8)
20,7	−5.14	0.55	27.86	0.981(2)
20,8	−0.638	0.053	8.788	0.961(6)
20,9	−0.114	0.008	3.302	0.892(39)
20,10	−0.02	0.00	1.37	0.80(10)
20,11	−0.01	0.00	0.61	0.44(24)

pends on factors that were not well known experimentally, such as the polarization direction of the stray electric field and the distribution of m_K levels contributing to the microwave signal. Simulations show that the differential shift rate is larger for stray fields polarized perpendicular to the microwave electric field and for large values of m_K relative to the stray field direction. In general, the shift rate is negative for both K levels and larger for the upper K level, indicating that the differential shifts would decrease the apparent K splitting as the data suggests. Since the approximate scaling of the Stark shifts is n^7, the shifts would be expected to be about a factor of 3 larger for $n=20$ than for $n=17$, also in agreement with the data pattern. The simulations indicate that the magnitude of the differential shift rates can be anywhere between zero and 30% of the average shift rate of the two K levels of common L, depending on the field polarization and the m_K distribution. The significance of these differential shifts is increased by the method that was used to determine the K splittings for high-L levels in Ref. [13]. For both $n=17$ and $n=20$, a single $\Delta L=1$, $\Delta K=0$ transition was observed at the lowest L studied, determining the K splitting directly in the lowest L levels, (17,6) and (20,7). The K splittings in higher L levels were then inferred by addition of $\Delta L=1$, $\Delta K=1$ resonance positions. As a result, any differential shifts accumulated toward the highest L. For example, in the $n=20$, $L=11$ level, the inferred K splitting could be expected to be smaller than the true splitting by between zero and 30% of the cumulative Stark shift of the $n=20$, $L=7$, 8, 9, 10, and 11 levels. Table VII shows both the Stark shifts of each L level, $\Delta\bar{E}_S$, and the cumulative Stark shift moving upwards from the lowest L level of each n, $\Delta\bar{E}_T$. These calculations assumed an average stray electric field squared of $0.0057(10)$ $(\text{V/cm})^2$, as reported in Ref. [13]. A rough estimate of the magnitude of differential shifts can be obtained by requiring consistency between the $n=17$ and $n=20$ measurements. This indicates a differential shift rate of approximately 15(8)% of the average Stark shift. Correction for this differential shift eliminates the disagreement between the highest L measurements and the extended model, while leaving the lower L measurements virtually unchanged.

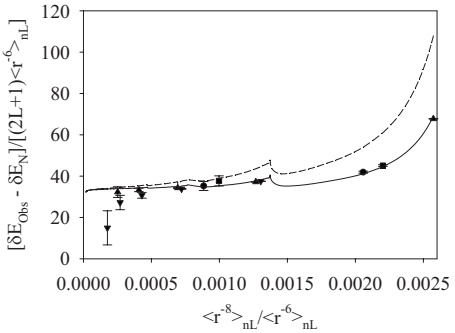

FIG. 2. Comparison of measured barium K splittings to second-order and extended theoretical models. The theory using the second-order model is shown with a dashed line, while the extended theory including the most important third- and fourth-order terms is shown with a solid line. Both theoretical calculations assume the matrix elements from Table I. The $n=9$ data are shown with circles, $n=10$ with squares, $n=17$ with triangles pointing up, and $n=20$ with triangles pointing down.

III. EXTRACTION OF TRANSITION STRENGTHS

Although the extended model generally agrees with measurements to a few percent after the differential Stark shift is taken into account, this represents a difference of many standard deviations for the most precise measurements. Estimates of terms not included here indicate that they are not large enough to account for this discrepancy. Changing the matrix elements themselves, however, is another way to alter the calculated K splittings. Since the K splittings result from a failure of cancellation between different terms in the second-order energy, as illustrated by Eqs. (13) and (14), the predicted splittings can be altered either by a common change in the magnitude of the two fine-structure matrix elements or by a change in their ratio. Thus, in order to extract the best estimates of transition strengths, the observations were fit by adjusting the size of the dipole and quadrupole contributions to the splittings by variable factors, while keeping the contributions of the third- and fourth-order terms constant. In addition, the fraction f_S, which represents the ratio between the differential Stark shift and the cumulative Stark shift $\Delta\bar{E}_T$, was included as a free parameter in the fit. This led to the fitting function

$$\delta E_{Obs} = A_1 \delta E_{DD} + A_2 \delta E_{QQ} + f_S \Delta\bar{E}_T + \delta E_{HO} + \delta E_N, \tag{23}$$

where δE_{Obs} is the reported splitting [13,14] and δE_{HO} and δE_N are fixed at the values indicated by Eqs. (19)–(22) using

TABLE VII. Comparison of the measured barium K splittings to the results of the fit from Eq. (23). Column 2 gives the Stark shift of each level, $\Delta\bar{E}_S$, assuming an average squared electric field of 0.0057 $(\mathrm{V/cm})^2$ [13] while column 3 shows the cumulative Stark shift, $\Delta\bar{E}_T$. The total theory, adjusted by the fitted factors A_1 and A_2, is shown in column 4. Column 5 shows the excess of the observed splittings over the normal magnetic splittings, corrected for the differential Stark shifts. The ratio of these observed values to the adjusted theory is shown in column 6. The $L=6$ splittings, indicated by an asterisk, were not used in the fit, but are included here for completeness. All values are in MHz.

nL	$\Delta\bar{E}_S$	$\Delta\bar{E}_T$	Total $\delta E'_{\mathrm{Theor.}}$	$\delta E_{Obs}-\delta E_N-f_S\Delta\bar{E}_T$	$\frac{\delta E_{Obs}-\delta E_N-f_S\Delta\bar{E}_T}{\delta E'_{\mathrm{Theor.}}}$
9,6*	0	0	714	733(9)	1.03(1)
9,7	0	0	140	145(9)	1.04(6)
10,6*	0	0	640	648(9)	1.014(9)
10,7	0	0	126	137(9)	1.09(7)
17,6*	−0.03	−0.03	272.67	263.37(10)	0.9659(4)
17,7	−0.060	−0.091	41.821	41.961(89)	1.003(2)
17,8	−0.10	−0.20	12.98	13.06(11)	1.006(9)
17,9	−0.16	−0.36	4.77	4.81(12)	1.01(3)
17,10	−0.23	−0.59	1.93	1.97(15)	1.02(8)
20,7	−0.202	−0.202	27.428	27.353(56)	0.997(2)
20,8	−0.360	−0.562	8.581	8.520(53)	0.993(6)
20,9	−0.59	−1.15	3.21	3.10(13)	0.96(4)
20,10	−0.90	−2.05	1.33	1.37(14)	1.03(11)
20,11	−1.28	−3.34	0.59	0.71(15)	1.19(25)

the matrix elements from Table I and known term energies [3]. The quantities δE_{DD} and δE_{QQ} are also calculated in this way from Eqs. (4) and (6), but their contributions to the splittings are adjusted by the variable parameters A_1 and A_2. Since the third- and fourth-order terms in δE_{HO} represent more than 30% of the total theory in $L=6$ levels, these states were not included in the fit. Fitting only the $L\geq 7$ states, the following parameters were returned:

$$A_1 = 0.968(10),$$

$$A_2 = 1.025(21),$$

$$f_S = 0.13(4),$$

and an excellent fit of all the data was obtained, as detailed in Table VII. Apparently, to correctly predict the K splittings, both contributions to the second-order energy, DD and QQ, should be slightly modified. It should be noted that an alternate fit including the $L=6$ states changes the resulting parameters by less than two standard deviations, giving confidence that the most significant terms in the extended theory have been included.

As stated before, the K splitting can be adjusted by varying either the common magnitude of the two fine-structure matrix elements or their ratio. This sensitivity to the ratio of matrix elements is a unique feature of the K splittings. In Fig. 3, the upward sloping solid lines show the range of quadrupole matrix elements that are consistent with the required increase of the QQ contribution to the K splittings. For comparison, Fig. 3 also shows the single point corresponding to the matrix elements of Table I and a dotted line representing the matrix element values consistent with the LS coupling ratio. The ranges of each matrix element allowed by the measured lifetimes of the $5D_{3/2}$ and $5D_{5/2}$ states are shown by dashed lines, with the area enclosed by the dashed ellipse representing the region where $\chi^2<1$ for these measurements. The downward sloping solid lines show an additional constraint corresponding to the measured quadrupole polarizability of the $6S_{1/2}$ state, obtained by fitting Rydberg fine-structure energies to the polarization model. Numerical

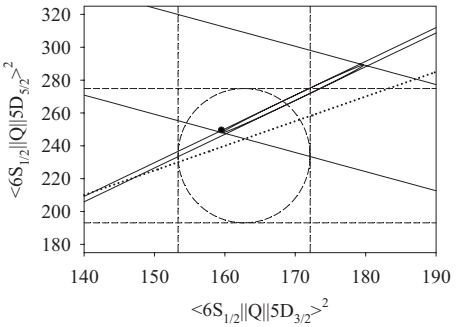

FIG. 3. Square of the quadrupole matrix elements connecting the Ba^+ ground state to the excited $5D_{3/2}$ state (horizontal axis) and the $5D_{5/2}$ state (vertical axis). The point shows the theoretical matrix elements from Table I while the dotted line represents the matrix element values consistent with the LS coupling ratio [Eq. (15)]. Vertical dashed lines show the range allowed by the $5D_{3/2}$ lifetime [11] while the horizontal dashed lines show the range allowed by the $5D_{5/2}$ lifetime [12]. Downward sloping solid lines show the range allowed by the quadrupole polarizability [14] while upward sloping lines show the range allowed by the fitted QQ contribution to the K splittings.

TABLE VIII. Limits on the electric-dipole and -quadrupole matrix elements and their ratios derived from the K splitting and polarizability measurements in barium Rydberg levels. All values are in atomic units.

Quantity	Expt.	(Expt.)/(Theor.)
$\langle 6S_{1/2}\|D\|6P_{1/2}\rangle$	3.327(7)	0.9974(21)
$\langle 6S_{1/2}\|D\|6P_{3/2}\rangle$	4.705(11)	0.9997(23)
Ratio	0.7071(7)	0.9977(10)
$\langle 6S_{1/2}\|Q\|5D_{3/2}\rangle$	13.0(4)	1.029(32)
$\langle 6S_{1/2}\|Q\|5D_{5/2}\rangle$	16.4(6)	1.038(39)
Ratio	0.796(9)	0.996(15)

details of the lifetime and polarization constraints are given in the Appendix. Since the polarizability is sensitive to the sum of the two matrix elements squared, it is relatively insensitive to the ratio of matrix elements. This is complementary to the dependence shown by the K splittings and together they determine constraints on the possible values of both matrix elements that are comparable in precision to those posed by the best lifetime measurements. The ellipse marked by the solid line represents the region where the sum of the χ^2 of the polarizability and K-splitting measurements is less than 1. Table VIII shows the corresponding limits placed on the quadrupole matrix elements and their ratio by the K splitting and polarizability measurements. The matrix elements are determined in this way to a precision of 3%–4% and are in full agreement with the theoretical values shown in Table I. The ratio between matrix elements is determined to a precision of about 1%, supporting the calculated 2% deviation of the ratio from the LS coupling value.

A similar analysis of the dipole matrix elements is shown in Fig. 4. The constraint posed by the required reduction of the DD contribution to the K splittings is shown, along with

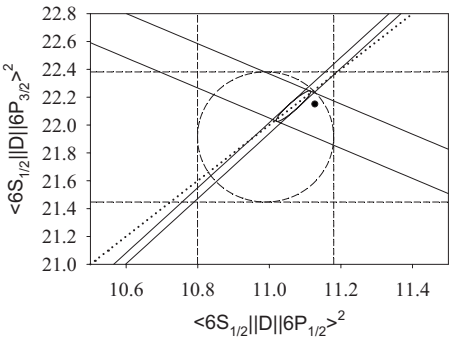

FIG. 4. Square of the dipole matrix elements connecting the Ba^+ ground state to the excited $6P_{1/2}$ state (horizontal axis) and the $6P_{3/2}$ state (vertical axis). The point shows the theoretical matrix elements from Table I while the dotted line represents the matrix element values consistent with the LS coupling ratio [Eq. (15)]. Vertical dashed lines show the range allowed by the $6P_{1/2}$ lifetime while the horizontal dashed lines show the range allowed by the $6P_{3/2}$ lifetime [13]. Downward sloping solid lines show the range allowed by the quadrupole polarizability [14] while upward sloping lines show the range allowed by the fitted DD contribution to the K splittings.

the calculated dipole matrix elements from Table I, the constraints posed by the measured lifetimes of the $6P_{1/2}$ and $6P_{3/2}$ levels, and the constraint posed by the precise measurement of the $6S_{1/2}$ dipole polarizability. In this case, the region of consistency with the two Rydberg measures is much smaller than the region limited by the two lifetime measurements. The Rydberg measurements determine the dipole matrix elements to a precision of about 0.2%, as shown in Table VIII, in good agreement with the theoretical values shown in Table I. The ratio between matrix elements is determined with precision of 0.1% and is completely consistent with the ratio expected for pure LS coupling, in contrast to the calculated matrix elements from Table I whose ratio differs from this value by 0.2%.

IV. CONCLUSIONS

An improved analysis of previously reported measurements of K splittings in barium Rydberg levels has resulted in precise experimental determinations of dipole and quadrupole matrix elements connecting the Ba^+ ground state to the lowest P and D levels. The results are in good agreement with matrix elements calculated using relativistic many-body perturbation theory. The result confirms the suggestion that K splittings could be a significant source of information about ionic transition strengths [8]. A particularly interesting aspect of the analysis is the emergence of complementarity between K splitting and polarizability measurements. Together, these two types of Rydberg spectroscopy appear to offer information that is comparable or better than information derived from precise lifetime measurements.

ACKNOWLEDGMENTS

We wish to thank W. G. Sturrus and Mariana Safronova for helpful discussions during the course of this work. This work was supported by the Chemical Sciences, Geosciences, and Biosciences Division of the Office of Basic Energy Sciences, Office of Science, U.S. Department of Energy.

APPENDIX

1. Energies

The excitation energies of the first four excited states of Ba^+ are [3]

$$5\ ^2D_{3/2}\text{:}4873.852\ \text{cm}^{-1},$$

$$5\ ^2D_{5/2}\text{:}5674.807\ \text{cm}^{-1},$$

$$6\ ^2P_{1/2}\text{:}20\ 261.561\ \text{cm}^{-1},$$

$$6\ ^2P_{3/2}\text{:}21\ 952.404\ \text{cm}^{-1}.$$

2. Lifetimes

The measured radiative lifetimes of each of these states are listed in Table II. These are compared to calculated lifetimes in Ref. [9], setting constraints on the matrix elements

considered here. For clarity, the following equations express the constraints, as derived from Ref. [9]:

$$\frac{1}{\tau_{6P_{1/2}}}(\mathrm{s}^{-1}) = 8.426\,67 \times 10^{6}\langle 6S_{1/2}\|\vec{D}\|6P_{1/2}\rangle^2 + 3.397\,74 \times 10^{7} = \frac{10^9}{7.90(10)}, \tag{A1}$$

$$\frac{1}{\tau_{6P_{3/2}}}(\mathrm{s}^{-1}) = 5.358\,63 \times 10^{6}\langle 6S_{1/2}\|\vec{D}\|6P_{3/2}\rangle^2 + 4.079\,61 \times 10^{7} = \frac{10^9}{6.32(10)}, \tag{A2}$$

$$\frac{1}{\tau_{5D_{3/2}}}(\mathrm{s}^{-1}) = 7.700\,17 \times 10^{-5}\langle 6S_{1/2}\|\vec{\vec{Q}}\|5D_{3/2}\rangle^2 = \frac{1}{79.8(46)}, \tag{A3}$$

$$\frac{1}{\tau_{5D_{5/2}}}(\mathrm{s}^{-1}) = 1.098\,51 \times 10^{-4}\langle 6S_{1/2}\|\vec{\vec{Q}}\|5D_{5/2}\rangle^2 + 5.544\,72 \times 10^{-3} = \frac{1}{32.0(6)}. \tag{A4}$$

The constant terms on the left-hand side of these expressions represent the portion of the decay rates due to transitions to states other than the $6\ ^2S_{1/2}$ ground state. Since these contribute less than about 30% to the total decay rate, their contribution to the uncertainty in the derived matrix elements is neglected. The resulting constraints are

$$\langle 6S_{1/2}\|\vec{D}\|6P_{1/2}\rangle = 3.315(29)\ \text{a.u.},\quad 0.9\%,$$

$$\langle 6S_{1/2}\|\vec{D}\|6P_{3/2}\rangle = 4.68(5)\ \text{a.u.},\quad 1.1\%,$$

$$\langle 6S_{1/2}\|\vec{\vec{Q}}\|5D_{3/2}\rangle = 12.8(4)\ \text{a.u.},\quad 2.9\%,$$

$$\langle 6S_{1/2}\|\vec{\vec{Q}}\|5D_{5/2}\rangle = 15.3(1.3)\ \text{a.u.},\quad 8.7\%.$$

3. Polarizabilities

The measured dipole and quadrupole polarizabilities are dominantly due to coupling to the $6p$ and $5d$ levels, respectively. However, as described in Ref. [9], there are also contributions from higher-excited levels, the core, and a valence-core counter term. Taking these additional contributions from Ref. [9], the resulting constraints on the matrix elements studied here are

$$\alpha_D(6\ ^2S_{1/2})(\text{a.u.}) = 3.610\,69\langle 6S_{1/2}\|\vec{D}\|6P_{1/2}\rangle^2 + 3.332\,58\langle 6S_{1/2}\|\vec{D}\|6P_{3/2}\rangle^2 + 10.15(53) = 123.88(5) \tag{A5}$$

and

$$\alpha_Q(6\ ^2S_{1/2})(\text{a.u.}) = 9.006\,21\langle 6S_{1/2}\|\vec{\vec{Q}}\|5D_{3/2}\rangle^2 + 7.735\,05\langle 6S_{1/2}\|\vec{\vec{Q}}\|5D_{5/2}\rangle^2 + 814 = 4420(250). \tag{A6}$$

Again, the constant terms on the left-hand side of the equations represent the contributions from higher-excited states and the Ba^{2+} core. For the dipole polarizability, the uncertainty in the polarizability of the core is estimated [9] to be 5%, or a factor of 10 larger than the experimental uncertainty, and this limits the precision with which the matrix elements are constrained by the measurement. For the quadrupole polarizability, the uncertainty in the calculation of the constant term is much smaller than the experimental uncertainty, so it has negligible effect on the constraint.

[1] B. Arora, M. S. Safronova, and C. W. Clark, Phys. Rev. A **76**, 064501 (2007).
[2] T. W. Koerber, M. Schacht, W. Nagourney, and E. N. Fortson, J. Phys. B **36**, 637 (2003).
[3] Yu. Ralchenko *et al.*, NIST Atomic Spectra Database (version 3.1.5), http://physics.nist.gov/asd3.
[4] R. E. Imhof and F. H. Read, Rep. Prog. Phys. **40**, 1 (1977).
[5] S. R. Lundeen, in *Advances in Atomic, Molecular, and Optical Physics*, edited by C. C. Lin and P. Berman (Academic Press, New York, 2005), Vol. 52, pp. 161–208.
[6] T. F. Gallagher, R. Kachru, and N. H. Tran, Phys. Rev. A **26**, 2611 (1982).
[7] E. L. Snow, R. A. Komara, M. A. Gearba, and S. R. Lundeen, Phys. Rev. A **68**, 022510 (2003).
[8] E. S. Shuman and T. F. Gallagher, Phys. Rev. A **74**, 022502 (2006).
[9] E. Iskrenova-Tchoukova and M. S. Safronova, Phys. Rev. A **78**, 012508 (2008).
[10] N. Yu, W. Nagourney, and H. Dehmelt, Phys. Rev. Lett. **78**, 4898 (1997).
[11] J. Gurell *et al.*, Phys. Rev. A **75**, 052506 (2007).
[12] E. H. Pinnington, R. W. Berends, and M. Lumsden, J. Phys. B **28**, 2095 (1995).
[13] E. L. Snow and S. R. Lundeen, Phys. Rev. A **76**, 052505 (2007).
[14] E. L. Snow, M. A. Gearba, R. A. Komara, S. R. Lundeen, and W. G. Sturrus, Phys. Rev. A **71**, 022510 (2005).
[15] R. A. Komara, W. G. Sturrus, D. H. Pollack, and W. R. Cochran, Phys. Rev. A **59**, 251 (1999).